

Mechanochemical synthesis and giant dielectric properties of $\text{CaCu}_3\text{Ti}_4\text{O}_{12}$

Mohamad M. Ahmad · Eman Al-Libidi ·
Abdullah Al-Jaafari · Syed Ghazanfar ·
Koji Yamada

Received: 13 September 2013 / Accepted: 3 January 2014 / Published online: 12 January 2014
© Springer-Verlag Berlin Heidelberg 2014

Abstract $\text{CaCu}_3\text{Ti}_4\text{O}_{12}$ powder has been synthesized by mechanochemical milling (C-m) and solid-state reaction (C-ssr) techniques. C-m powder has a grain size of ~ 24 nm as determined from X-ray diffraction and FE-SEM measurements. The grain size of C-m ceramics has increased to $20 \mu\text{m}$ compared to a size of $3 \mu\text{m}$ for C-ssr ceramics after sintering at $1,050^\circ\text{C}$ for 10 h. Giant dielectric constant was observed in both ceramics with that of C-m larger than that of C-ssr. Impedance results show that the grain conductivity of C-m is more than two orders of magnitude lower than that of C-ssr, whereas its grain boundary conductivity is larger than that of C-ssr. These results are supported by the EDX results that show Cu-enriched grain boundaries in C-m ceramics.

1 Introduction

$\text{CaCu}_3\text{Ti}_4\text{O}_{12}$ (CCTO) ceramics have attracted great research interests in the past years due to their unusually giant dielectric constant (GDC) properties [1–18]. This material shows a dielectric constant value ϵ' of 10^4 – 10^5

that is almost independent of temperature and frequency over wide ranges. The GDC properties make CCTO a potential candidate in microelectronic applications such as capacitive and memory devices components. CCTO exhibits cubic perovskite-like structure with space group $Im\bar{3}$, and no indications of structural phase transition have been observed in the 100–600 K temperature range [1]. Therefore, the GDC in CCTO ceramics is not due to ferroelectric characteristics of the material. The dielectric behavior of CCTO depends on the method of preparation and processing conditions such as the sintering temperature, dwelling time and the atmosphere [7–18]. CCTO powder has been synthesized by different techniques, mostly by multi-step solid state reaction technique where the starting materials are mixed and calcined at high temperatures [4–9]. Sol-gel, polymerization, molten salt and other wet chemical methods have also been used to synthesize CCTO powder [10–18]. In the above synthesis methods different nano- and micro-sized CCTO powders were obtained, which transform to micro-sized CCTO ceramics after sintering the compacted powder at high temperature (mostly between $1,000$ and $1,125^\circ\text{C}$) for several hours (between 3 and 48 h). In these ceramics, the grain size is usually range between 1 and $300 \mu\text{m}$. The dielectric constant of the resultant CCTO ceramics has different values from few hundred up to 10^5 .

Mechanochemical synthesis is considered a complete general method of producing almost all forms of materials in the nanosize. The advantages of the mechanical milling are; (1) almost every material is accessible, (2) large amounts can be produced, and (3) skips intermediate temperature calcination steps that are usually performed in solid state reaction technique, leading to a simpler processes. Therefore, mechanochemical milling technique has been used for the preparation of a large

M. M. Ahmad (✉) · E. Al-Libidi · A. Al-Jaafari · S. Ghazanfar
Department of Physics, College of Science, King Faisal
University, Al-Ahsaa 31982, Saudi Arabia
e-mail: mmohamad@kfu.edu.sa

M. M. Ahmad
Department of Science and Mathematics, College of Education,
Assiut University in The New Valley, El-Kharga 72511, Egypt

K. Yamada
Department of Applied Molecular Chemistry, College of
Industrial Technology, Nihon University, Narashino,
Chiba 275-8575, Japan

varieties of materials including; ionic conductors, ferroelectrics, semiconducting oxides, etc. [19–23]. Moreover, using hard materials like tungsten carbide, for example, for the vial and balls we can overcome the disadvantage of the abrasion of the milling media and the contamination that may occur. Mechanochemical synthesis of CCTO, without the need of calcination steps, has been reported in the literature [24–26]. In these reports, CCTO has been synthesized from $\text{CaO}/\text{CaCO}_3/\text{Ca}(\text{OH})_2$, CuO and TiO_2 using stainless steel vials and balls. The milling time needed to form CCTO phase is different and range from 30 to 60 h [24], 14 h [25], and more than 200 h [26]. The grain size in the product CCTO powder has an average value of 17–28 nm [24–26]. However, until now there are no reports on the microstructure and dielectric properties of CCTO ceramics prepared from mechanosynthesized powder. Therefore, the aim in the present work is to synthesize CCTO nanopowder by mechanochemical milling and study the microstructure of its corresponding ceramics. Moreover, the dielectric, transport and relaxation properties will be investigated through impedance spectroscopy measurements.

2 Experiment

Nanocrystalline $\text{CaCu}_3\text{Ti}_4\text{O}_{12}$ was synthesized by mechanochemical synthesis at RT using stoichiometric proportions of CaCO_3 (99 %), CuO (99.99 %) and TiO_2 (99.9 %) all from Sigma-Aldrich. The milling process was performed in Fritsch P-7 premium line machine using a 45-ml WC pot and 15 WC balls of 10-mm diameter, where the balls to powder mass ratio was 8:1. The milling process continued for 30 h with a rotation speed of 500 rpm in the first 5 h and 400 rpm for the rest of the milling time. For comparison CCTO powder was also synthesized by solid-state reaction where the mixed powder of starting materials was grounded in agate mortar, calcined at 900 °C for 10 h, re-grounded and calcined again at 1,000 °C for 10 h. Dense CCTO ceramics were obtained from the two powder sources by sintering at 1,050 °C for 10 h. The two ceramic samples will be called C-m (from mechanosynthesized powder) and C-ssr (from the solid state reaction powder source). Materials characterization was performed by X-ray diffraction and field-emission scanning electron microscope. For impedance measurements the studied ceramics were painted by silver paste and fired at 400 °C for 1 h. Impedance measurements were conducted for C-m and C-ssr samples in the 120–500 K temperature range over the 5 Hz–5 MHz frequency range using Hioki IM3570 LCR meter.

3 Results and discussion

Figure 1a and b shows the room temperature XRD patterns of CCTO powders synthesized by solid-state reaction and mechanochemical milling, respectively. This figure indicates that pure CCTO cubic phase is obtained in the two powder sources without noticeable secondary phases. However, XRD peaks of C-m material are considerably broad compared to the sharp peaks of C-ssr material. The broadening is mainly due to the reduction of the crystallite size of the product material due to the mechanochemical synthesis process. The crystallite size could be estimated from the full width at half maximum (FWHM) of the XRD peaks using Scherrer formula;

$$d = \frac{k\lambda}{\beta \cos \theta}, \quad (1)$$

where d is the crystallite size, $k = 0.89$, β is the line's FWHM, θ is the Bragg angle and λ (0.154 nm) is wavelength of the X-ray radiation. The FWHM of XRD peaks was corrected using Si as a standard. The estimated crystallite size is in the range of 24 nm. This result is supported

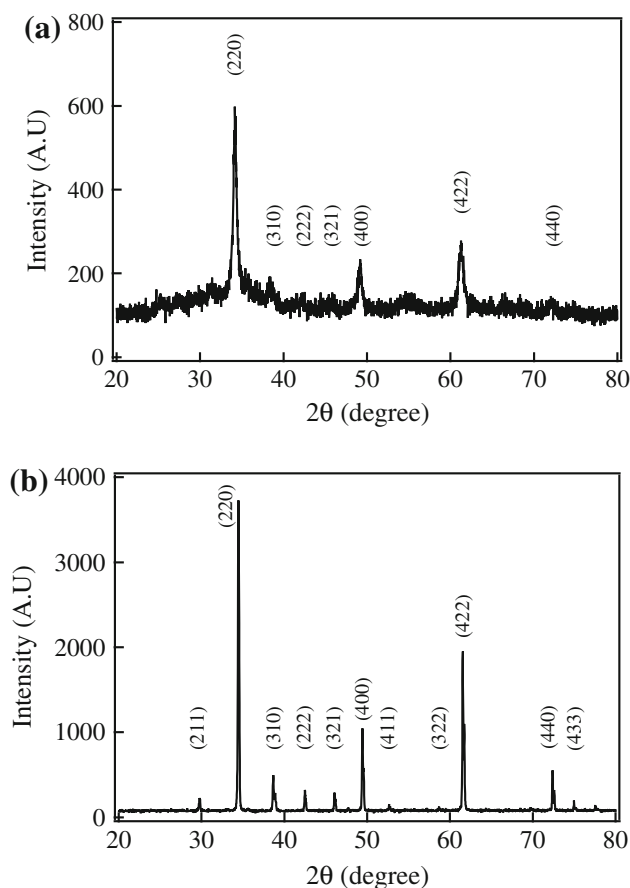


Fig. 1 XRD patterns of CCTO powder synthesized by **a** mechanochemical milling and **b** solid-state reaction

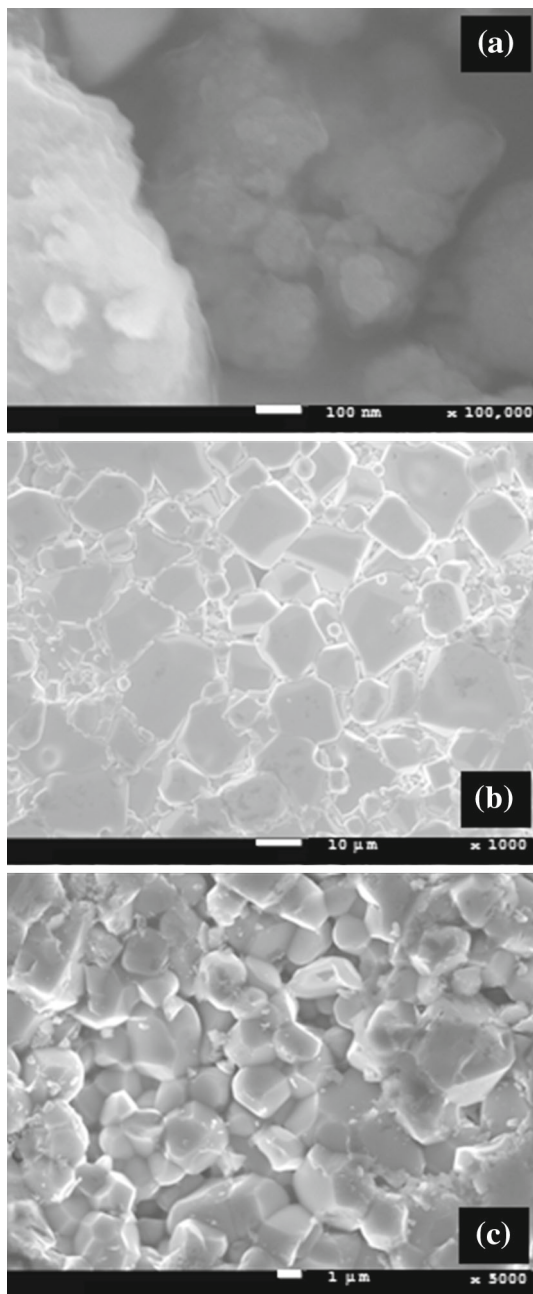


Fig. 2 FE-SEM of **a** CCTO mechanosynthesized powder, **b** C-m ceramics and **c** C-ssr ceramics

by the FE-SEM micrograph in Fig. 2a. This figure shows very fine agglomerations of about 100-nm size that include smaller grains of 20–30 nm. The observed XRD pattern and the calculated crystallite size of C-m powder in the current work agree with the results reported previously for CCTO powder prepared by mechanical milling [24–26]. The grain size of the C-m sintered ceramics is increased considerably after sintering at 1,050 °C for 10 h as shown in Fig. 2b. The grain size of C-m ceramics is not homogeneous where a majority of large grains of 20- μm size are

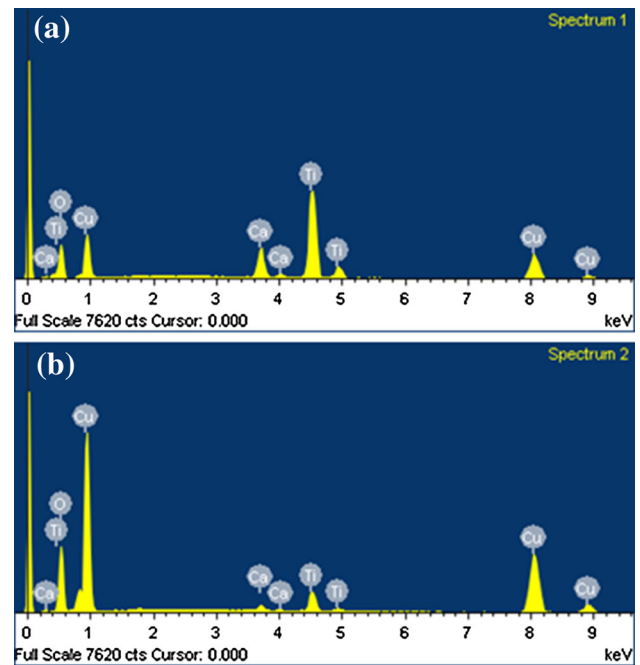


Fig. 3 EDX spectra of grain **(a)** and grain boundary **(b)** of C-m ceramics

Table 1 Element percentage at the grains and grain boundaries in C-m ceramics as determined from EDX spectra

	At % (grains)	At % (gain boundary)
O	66.21	63.47
Ca	4.40	1.02
Ti	16.95	3.76
Cu	12.44	31.75

observed with the presence of smaller grains of about 5- μm size. Moreover, thick Cu-rich intergranular phase is observed. Meanwhile, C-ssr ceramics sintered at the same conditions have homogenous microstructure with an average grain size of $\sim 3 \mu\text{m}$ as could be seen in Fig. 2c. These results suggest that the mechanosynthesis of CCTO enhanced the sinterability of the product nanopowder that leads to ceramics with larger grain size compared to the solid-state reaction technique. The composition of the grain and grain boundary of C-m ceramics was determined by EDX measurements. The EDX spectra of the grain and grain boundary phases of C-m ceramics are shown in Fig. 3 and the corresponding data are summarized in Table 1.

The frequency dependence of the dielectric constant ϵ' of C-m and C-ssr ceramics is shown in Fig. 4a and b, respectively, at selected temperatures. Moreover, Fig. 4c shows the frequency dependence of the dielectric constant for the two samples at RT. Both samples show large ϵ' plateau at low frequencies, followed by a large drop of the value of ϵ' to the bulk value at high frequency. The plateau

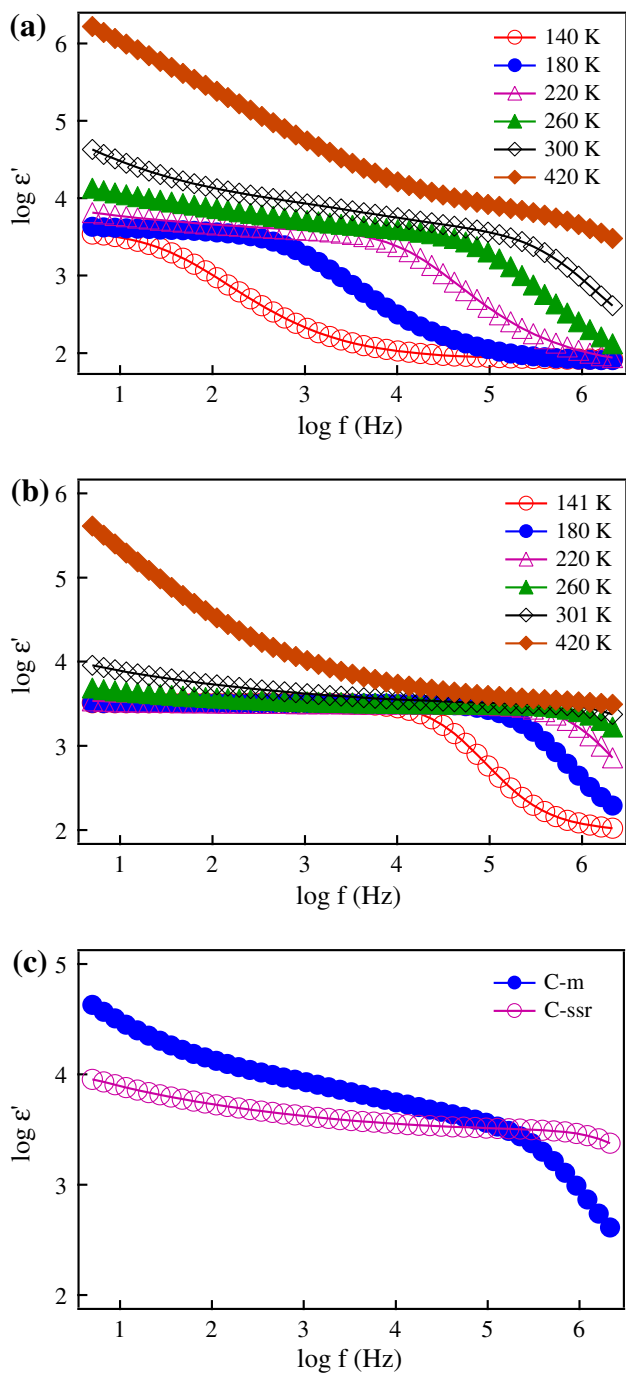


Fig. 4 Frequency dependence of ϵ' at selected temperatures for **a** C-m and **b** C-ssr ceramics. **c** Shows the frequency dependence of ϵ' of the two samples at RT for comparison

region expands to the high-frequency region with increasing temperature. However, pronounced differences exist between the two samples. (1) The plateau dielectric constant of C-m sample (4.1×10^3) is larger than that of C-ssr (3.2×10^3) sample. This could also be observed in Fig. 5, which shows the Cole–Cole plots of the dielectric constant of the two samples at 200 K. (2) The value of the bulk

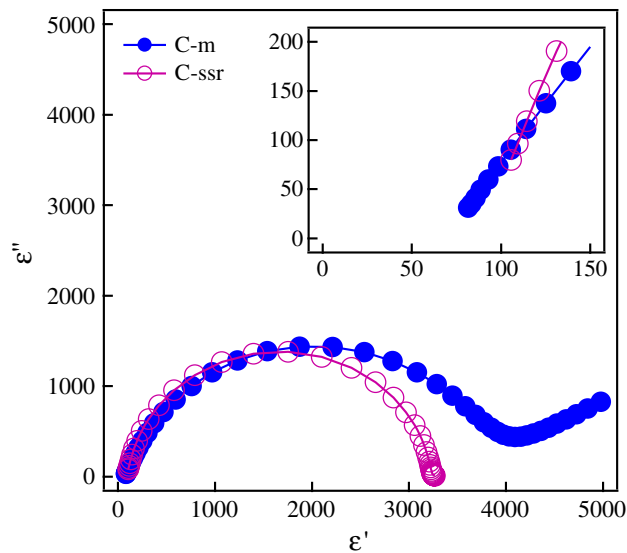


Fig. 5 Cole–Cole plots of the dielectric constant of C-m and C-ssr ceramics at 200 K. The inset shows a magnification of the high frequency part

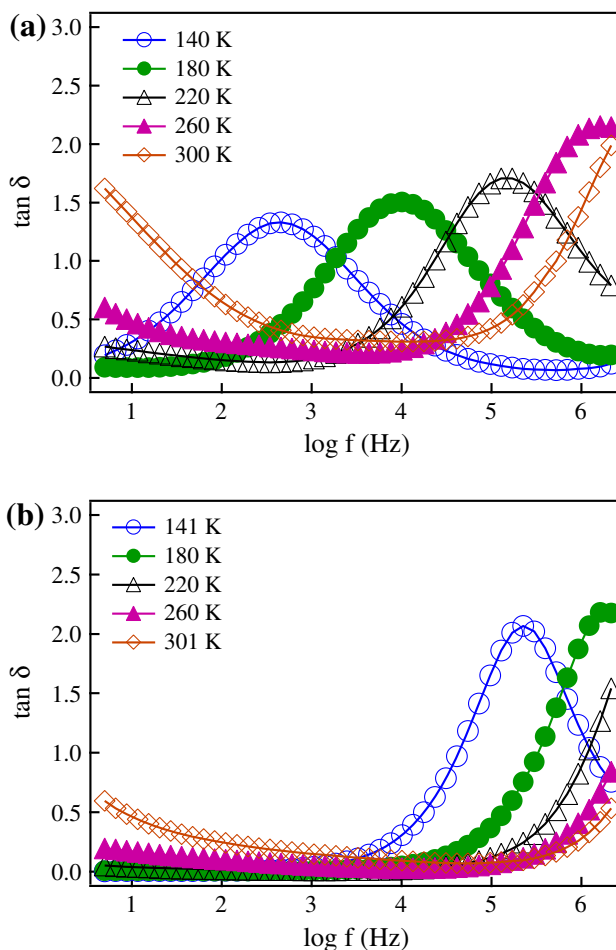


Fig. 6 Frequency dependence of $\tan \delta$ of **a** C-m and **b** C-ssr ceramics at selected temperatures

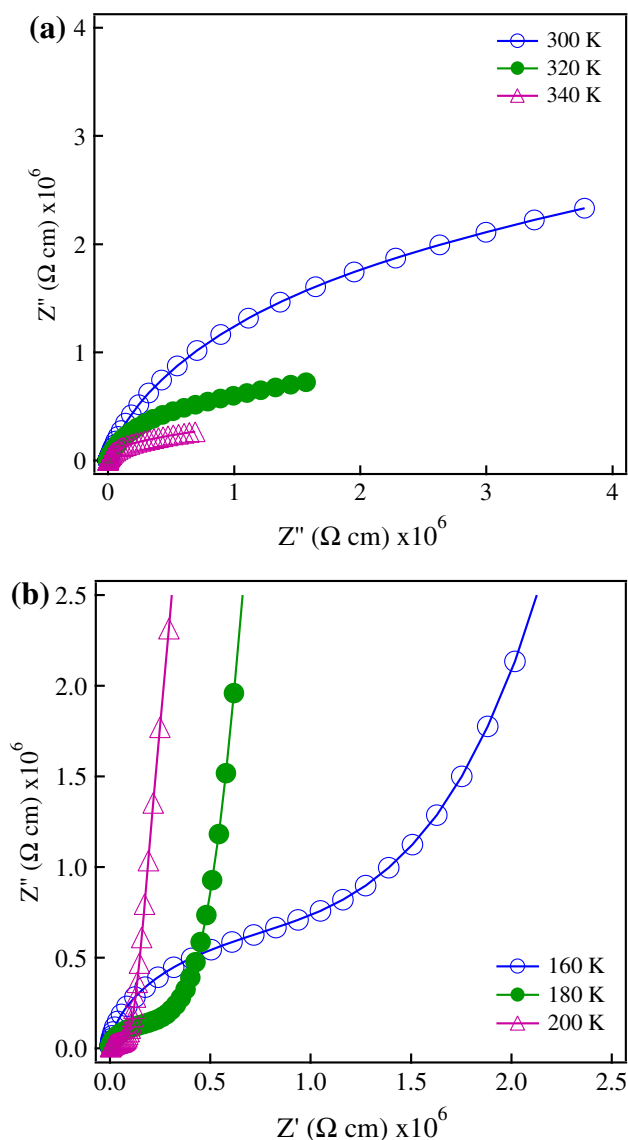


Fig. 7 **a** Complex plane diagrams of the grain boundary impedance of C-m ceramics at *selected temperatures*, and **b** shows the grain impedance at *low temperatures and high frequency*

dielectric constant of C-ssr (~ 100) is larger than that of C-m (~ 80) ceramics as seen from the inset of Fig. 4. (3) The drop of ϵ' to the bulk value for C-m sample occurs at much lower frequency than C-ssr ceramics at the same temperature. The corresponding frequency dependence of $\tan \delta$ for C-m and C-ssr is shown in Fig. 6. One relaxation peak is observed in this figure which is related to the grain boundary relaxation process. However, there is large difference of the relaxation frequency for C-m and C-ssr ceramics.

It is established in the literature that the giant values of ϵ' accompanied by a strong Maxwell–Wagner (M–W) relaxation mode are due to electrical heterogeneity of the

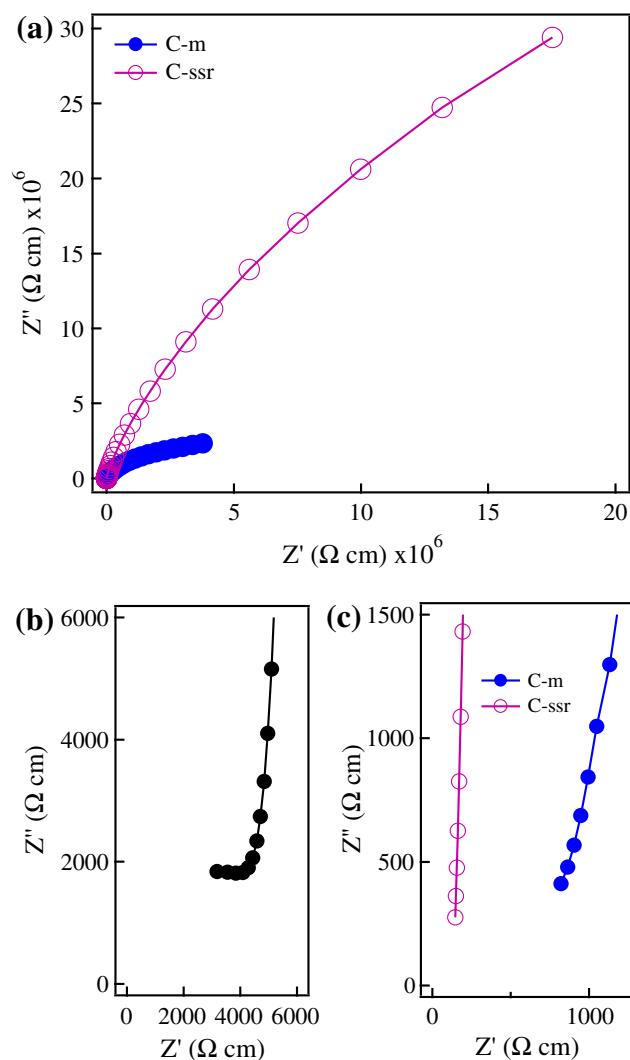


Fig. 8 **a** Comparison of the complex impedance diagram of C-m and C-ssr ceramics at RT indicating a very high grain boundary impedance of C-ssr compared to C-m ceramics. **b** Shows the grain impedance of C-ssr ceramics at 160 K and **c** shows the grain impedance of the two samples at RT

materials, leading to internal barrier layer capacitance (IBLC) effects, where polarization effects at insulating grain boundaries between semiconducting grains generate giant values of ϵ' [4–18, 27]. Therefore, the GDC properties of the current materials could be understood from their electrical behavior. Previous studies indicated that CCTO ceramics have semiconducting grains with resistivity $R_g \sim 10\text{--}100 \Omega \text{ cm}$ and insulating grain boundaries with $R_{gb} \sim 0.1\text{--}10 \text{ M}\Omega \text{ cm}$ at room temperature [27]. We show in Fig. 7 the complex plane plots of the resistivity of C-m ceramics at selected temperatures. The grain resistivity contribution is observed as a semicircle at low temperatures and high frequency with R_g value of about $1.5 \text{ M}\Omega \text{ cm}$ at 160 K (see Fig. 7b) that decreases to

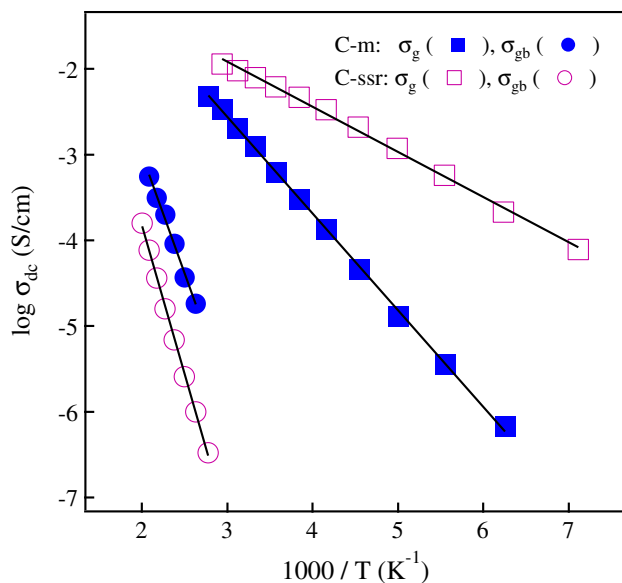
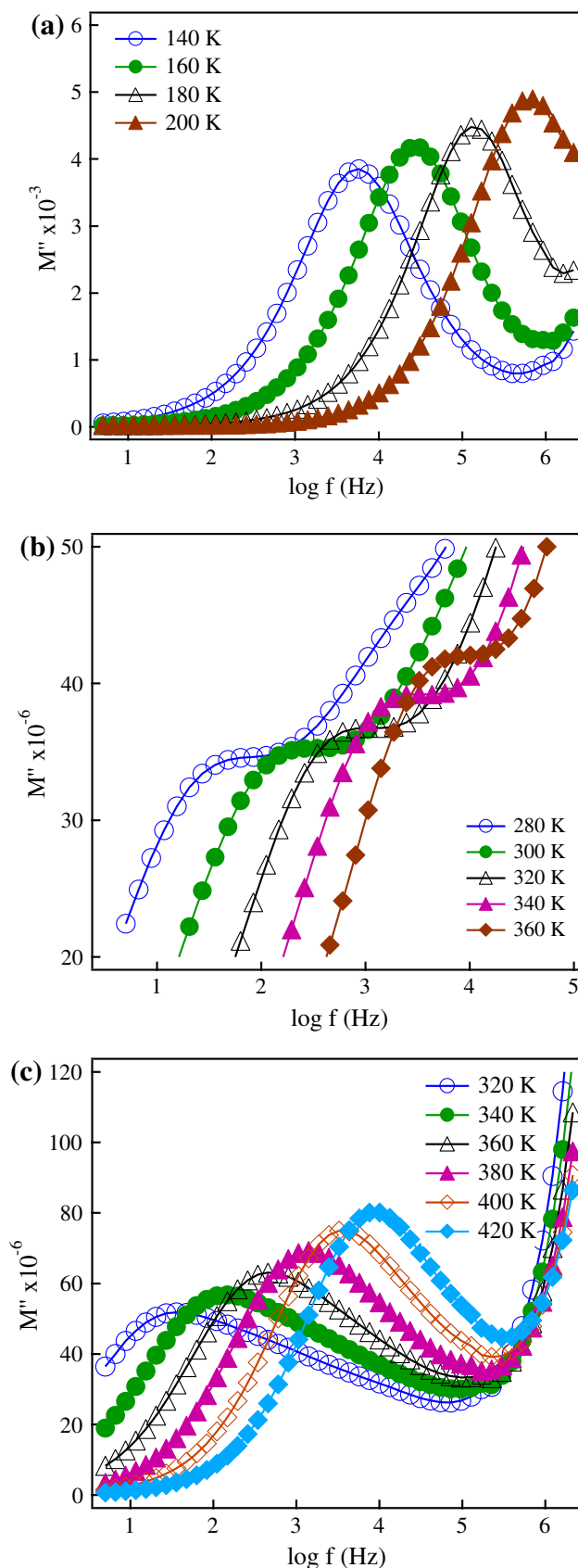


Fig. 9 Temperature dependence of the grain and grain boundary conductivity of C-m and C-ssr ceramics

800 Ω cm at RT (see Fig. 8c). These values of R_g are much larger than the R_g values of C-ssr ceramics of 4.27 k Ω cm and 125 Ω cm at 160 K and RT, respectively, (see Fig. 8b, c). On the other hand, grain boundary resistivity of C-m ceramics is more than one order of magnitude lower than that of C-ssr ceramics. At 380 K, for example, R_{gb} has values of 55 k Ω cm and 1 M Ω cm for C-m and C-ssr ceramics, respectively.

The temperature dependence of the grains and grain boundaries conductivity is illustrated in Fig. 9. It is observed from this figure that the grain conductivity of C-m ceramics is more than two orders of magnitude lower than that of C-ssr ceramics at low temperatures. On the other hand, the grain boundary conductivity of C-m ceramics is more than one order of magnitude larger than that of C-ssr ceramics. The values of the activation energy of the conduction processes are 0.224 and 0.104 eV for the grain conduction of the C-m and C-ssr ceramics, respectively, and 0.55 and 0.68 eV for the grain boundary conduction of C-m and C-ssr ceramics, respectively. Reduction of the grain conductivity associated with an increase of its activation energy in CCTO ceramics was reported for doped CCTO with different metal dopants such as Mn [28, 29]. The conductivity behavior of the grains and grain boundaries are related to the composition of the bulk and grain boundary phases of the ceramics. The

Fig. 10 Modulus spectra corresponding to **a** the grain and **b** grain boundary effects of C-m ceramics. **c** Shows the spectra corresponding to grain boundary effects of C-ssr ceramics



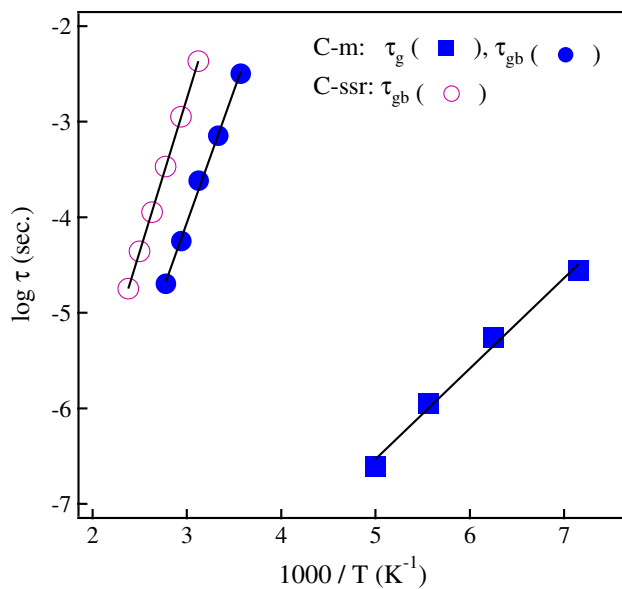


Fig. 11 Temperature dependence of the relaxation time determined from the modulus spectra

EDX spectra in Fig. 3 and the corresponding data in Table 1 of C-m ceramics show that the Ca/Cu ratio in the grains is 1:2.83, which is very close to the stoichiometric ratio 1:3 in CCTO. However, Ca/Cu ratio in the grain boundaries is 1:31, indicating a Cu rich/Ca and Ti deficient grain boundaries in C-m ceramics. Although the semi-conduction of grains and resistance of grain boundaries decrease in C-m ceramics, the grain conductivity is still three orders of magnitude larger than that of grain boundaries and the IBLC effect still valid leading to GDC. It is noteworthy to mention that CCTO nanoceramics prepared by spark plasma sintering at 975 °C of the mechano-synthesized powder have different microstructure and transport properties, where the grain size is limited to 200 nm and the grain conductivity is three orders of magnitude larger than that of C-m ceramics [30]. These results clearly indicate that the microstructure, transport and dielectric properties of CCTO ceramics depend strongly on the synthesis route and sintering technique and conditions.

The relaxation properties of the current materials could be studied through the frequency dependence of the electric modulus. The spectra of the imaginary part of the electric modulus M'' at selected temperatures are shown in Fig. 10 for C-m and C-ssr ceramics. For C-ssr ceramics one relaxation peak is observed that shifts to higher frequency with increasing temperature. This relaxation peak corresponds to the grain boundary effect in the material, whereas the relaxation peak of the grain effect could be observed at lower temperatures than the available temperature window in our impedance measurements. Due to

the lower grain conductivity of C-m ceramics two relaxation processes for grain and grain boundary effects could be observed for this material. The relaxation time is determined from the peak frequency in Fig. 10 and the associated temperature dependence is shown in Fig. 11. The activation energy of the relaxation processes is 0.188 eV for the grain relaxation of C-m ceramics and 0.55 and 0.64 eV for the grain boundary relaxation process of C-m and C-ssr ceramics, respectively. These values of the activation energies agree with those of the conduction processes.

4 Conclusions

Nanocrystalline powder of $\text{CaCu}_3\text{Ti}_4\text{O}_{12}$ has been synthesized by mechanochemical milling at room temperature without any heat treatment steps with grain size of 24 nm. The grain size of the corresponding ceramics increased considerably to 20 μm after sintering at 1,050 °C for 10 h. C-m ceramics show GDC larger than that of C-ssr ceramics. Impedance results show lower grain conductivity and higher grain boundary conductivity of C-m ceramics compared to C-ssr ceramics. These features are due to the Cu-rich grain boundary region. The current results along with those of spark plasma sintered ceramics indicate that the microstructure, transport and dielectric behavior of CCTO depend strongly on the synthesis route and sintering conditions.

Acknowledgments MMA acknowledges the financial support from NSTIP program (Grant No. 10–NAN1095–06) funded by King Abdulaziz City for Science and Technology (KACST).

References

1. M.A. Subramanian, D. Li, N. Duan, B.A. Reisner, A.W. Sleight, *J. Solid State Chem.* **151**, 323 (2000)
2. A.P. Ramirez, M.A. Subramanian, M. Gardel, G. Blumberg, D. Li, T. Vogt, S.M. Shapiro, *Solid State Commun.* **115**, 217 (2000)
3. S.Y. Chung, *Appl. Phys. Lett.* **87**, 052901 (2005)
4. T.T. Fang, W.J. Lin, C.Y. Lin, *Phys. Rev. B* **76**, 045115 (2007)
5. S.Y. Chung, I.D. Kim, S.J.L. Kang, *Nat. Mater.* **3**, 774 (2004)
6. P. Fiorenza, R.L. Nigro, C. Bongiorno, V. Raineri, M.C. Ferrarrelli, D.C. Sinclair, A.R. West, *Appl. Phys. Lett.* **92**, 182907 (2008)
7. T.B. Adams, D.C. Sinclair, A.R. West, *Phys. Rev. B* **73**, 094124 (2006)
8. T.B. Adams, D.C. Sinclair, A.R. West, *J. Am. Ceram. Soc.* **89**, 3129 (2006)
9. R. Yu, H. Xue, Z. Cao, L. Chen, Z. Xiong, *J. Eur. Ceram. Soc.* **32**, 1245 (2012)
10. M.A. de la Rubia, P. Leret, J. de Frutos, J.F. Fernandez, *J. Am. Ceram. Soc.* **95**, 1866 (2012)
11. D.L. Sun, A.Y. Wu, S.T. Yin, *J. Am. Ceram. Soc.* **91**, 169 (2008)
12. P. Jha, P. Arora, A.K. Ganguli, *Mater. Lett.* **57**, 2443 (2003)

13. V. Brizé, G. Gruener, J. Wolfman, K. Fatyeyeva, M. Tabellout, M. Gervais, F. Gervais, *Mater. Sci. Eng. B* **149**, 135 (2006)
14. J.J. Liu, Y.C. Sui, C.G. Duan, W.N. Mei, R.W. Smith, J.R. Hardy, *Chem. Mater.* **18**, 3879 (2006)
15. B.A. Bender, M.-J. Pan, *Mater. Sci. Eng. B* **117**, 339 (2005)
16. Y. Huang, L. Liu, D. Shi, S. Wu, S. Zheng, L. Fang, C. Hu, B. Elouadi, *Ceram. Inter.* **39**, 6063 (2013)
17. N. Banerjee, S.B. Krupanidhi, *J. Alloy Compd.* **509**, 4381 (2011)
18. B.P. Zhu, Z.Y. Wang, Y. Zhang, Z.S. Yu, J. Shi, R. Xiong, *Mater. Chem. Phys.* **113**, 746 (2009)
19. B. Ruprecht, M. Wilkening, S. Steuernagel, P. Heitjans, *J. Mater. Chem.* **18**, 5412 (2008)
20. M.M. Ahmad, Y. Yamane, K. Yamada, *Mater. Sci. Eng. B* **178**, 965 (2013)
21. T. Hungria, M. Alguero, A. Castro, *Chem. Mater.* **18**, 5370 (2006)
22. J. Lu, K.M. Ng, S. Yang, *Ind. Eng. Chem. Res.* **47**, 1095 (2008)
23. J. Huang, J.A. Moore, J.H. Acquaye, R.B. Kaner, *Macromolecules* **38**, 317 (2005)
24. A.F.L. Almeida, R.S. de Oliveira, J.C. Goes, J.M. Sasaki, A.G.S. Filho, J.M. Filho, A.S.B. Sombra, *Mater. Sci. Eng. B* **96**, 275 (2002)
25. S.K. Manik, S.K. Pradhan, *Physica E* **33**, 160 (2006)
26. M. Alizadeh, H.A. Ardakani, R. Amini, M.R. Ghazanfari, M. Ghaffari, *Ceram. Inter.* **39**, 3307 (2013)
27. T.B. Adams, D.C. Sinclair, A.R. West, *Adv. Mater.* **14**, 1321 (2002)
28. M. Li, A. Feteira, D.C. Sinclair, A.R. West, *Appl. Phys. Lett.* **88**, 232903 (2006)
29. Y.H. Lin, W. Deng, W. Xu, Y. Liu, D. Chen, X. Zhang, C.W. Nan, *Mater. Sci. Eng. B* **177**, 1773 (2012)
30. M.M. Ahmad, *Appl. Phys. Lett.* **102**, 232908 (2013)